PROCEEDINGS OF SPIE

SPIEDigitalLibrary.org/conference-proceedings-of-spie

Combined optical coherence tomography and light sheet fluorescence microscopy for embryonic imaging

Md Mobarak Karim, Ruijiao Sun, Behzad Khajavi, Manmohan Singh, Harshdeep S. Chawla, et al.

Md Mobarak Karim, Ruijiao Sun, Behzad Khajavi, Manmohan Singh, Harshdeep S. Chawla, Yogeshwari S. Ambekar, Alexander W. Schill, David Mayerich, Mary E. Dickinson, Kirill V. Larin, "Combined optical coherence tomography and light sheet fluorescence microscopy for embryonic imaging," Proc. SPIE 11952, Multimodal Biomedical Imaging XVII, 1195202 (2 March 2022); doi: 10.1117/12.2610091



Event: SPIE BiOS, 2022, San Francisco, California, United States

Combined optical coherence tomography and light sheet fluorescence microscopy for embryonic imaging

Md Mobarak Karim¹, Ruijiao Sun², Behzad Khajavi¹, Manmohan Singh¹, Harshdeep S. Chawla¹, Yogeshwari S. Ambekar¹, Alexander W. Schill¹, David Mayerich², Mary E. Dickinson³, and Kirill V. Larin^{1,3,*}

¹Department of Biomedical Engineering, University of Houston, Houston, TX, USA
²Department of Electrical and Computer Engineering, University of Houston, Houston, TX, USA
³Department of Molecular Physiology and Biophysics, Baylor College of Medicine, Houston, TX, USA

ABSTRACT

Optical coherence tomography (OCT) and light sheet fluorescence microscopy (LSFM) are well-established imaging techniques preferred in developmental biology, e.g., embryonic imaging. However, each technique has its own drawbacks, such as resolution and molecular specificity with OCT and field-of-view (FOV) and speed with LSFM. To overcome these limitations for small animal embryo imaging, we have developed a co-aligned multimodal imaging system combining OCT and LSFM. The OCT probe and LSFM excitation beams were combined and scanned with a galvanometer-mounted mirror through the same objective lens. The light sheet thickness was \sim 13 μ m. The LSFM collection arm consisted of a 0.8 numerical aperture water immersion objective, tube lens, and CCD camera, resulting in a transverse resolution of \sim 2.1 μ m. The OCT system was based on a 100 kHz swept-source laser with a central wavelength of 1050 nm and had a lateral resolution of \sim 15 μ m and an axial resolution of \sim 7 μ m. Images of fluorescent microbeads and a fluorescent-tagged mouse embryo at gestational day 9.5 showed the capabilities of the multimodal imaging system. Since the OCT system and LSFM system were co-aligned, image registration was straightforward and enabled high-throughput multimodal imaging without the need for complex registration techniques.

Keywords: Light Sheet Fluorescence Microscopy, Optical Coherence tomography, Multimodal imaging, Embryonic imaging

1. INTRODUCTION

Due to the biological similarities to humans, the mouse is a widely used model for mammalian developmental research [1]. For example, numerous genetically engineered mouse models are commonly used for simulating and analyzing human pathologies [2]. Recent advancements have provided deep insight into understanding these pathologies' genetic and developmental origin [3, 4]. Moreover, several optical imaging techniques have made it possible to visualize developmental processes at cellular, tissue, and organ scales to correlate with genetic information [5]. A wide range of imaging techniques has been developed to study mouse embryonic development, such as ultrasound biomicroscopy (UBM) [6], optical projection tomography (OPT) [7], micro magnetic resonance imaging (micro MRI) [8], and micro computed tomography (micro CT) [9]. UBM has a spatial resolution of \sim 50 μ m using high frequency ultrasound between 40 and 100 MHz [8]. Micro MRI is also capable of sub-millimeter resolution (25 \sim 100 μ m) but requires long acquisition times to achieve such resolution [8]. Micro CT has high similar high resolution but utilizes ionizing radiation and requires fixatives and external contrast agents for murine embryonic imaging [9]. OPT can acquire high resolution images (sub-micron resolution) of cleared and fixed samples, which restricts live imaging [7].

Optical coherence tomography (OCT) was initially developed for applications in ophthalmology, but it has proven itself as a powerful method for developmental biology [10-12]. OCT works on the principle of low coherence interferometry, which enables noninvasive, high speed volumetric imaging with no exogeneous contrast agents and high contrast. OCT can achieve

Corresponding Author * klarin@uh.edu

Multimodal Biomedical Imaging XVII, edited by Fred S. Azar, Xavier Intes, Qianqian Fang Proc. of SPIE Vol. 11952, 1195202 ⋅ © 2022 SPIE ⋅ 1605-7422 ⋅ doi: 10.1117/12.2610091

micrometer-scale spatial resolution with a penetration depth of a few millimeters within highly scattered tissues [13]. Since OCT is noninvasive and relies on backscattered light, and it can be used to image live samples. However, OCT lacks molecular specificity and cannot approach the spatial resolution of microscopy techniques.

Several fluorescence imaging techniques offer biochemical and molecular information with high resolution (sub-micron resolution). Among them, light-sheet fluorescence microscopy (LSFM) overcomes the limitation of conventional fluorescence microscopy for developmental biology [14]. LSFM, also known as selective plane illumination microscopy (SPIM), uses a thin plane of illumination, also called the light-sheet, and image acquisition is perpendicular to the illumination plane [15]. Since planar illumination minimizes photobleaching and phototoxicity as opposed to point-wise illumination, LSFM has become a preferred tool of choice for three-dimensional imaging in developmental biology [16]. However, it can still induce photodamage, and samples are commonly embedded in optically clear semi-solids, e.g., agarose, agar, and gelatin, to eliminate bulk motion, introducing noise and limiting live imaging [16].

In this work, we developed a co-aligned multimodal imaging system combining OCT and LSFM to overcome the individual drawbacks for small animal embryo imaging. Since both systems were co-planar and shared optical components, image registration was trivial.

2. MATERIALS AND METHODS

2.1 Experimental Setup

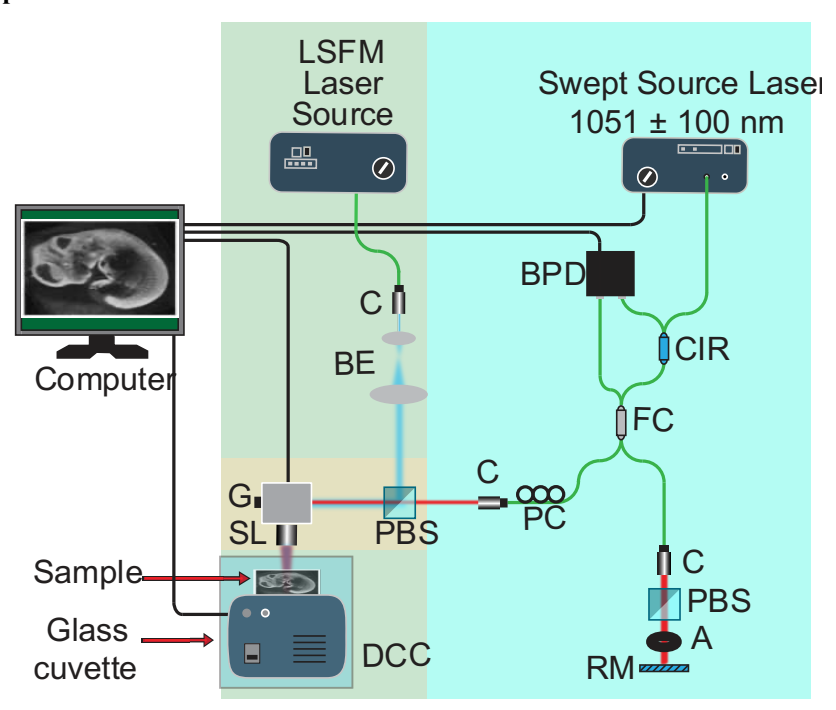


Figure 1. The schematic of the combined OCT+ LSFM system. A: Aperture, BPD: Balanced Photo Detector, BE: Beam Expander, BS: Beam Splitter, C: Collimator, CCD: Charged Couple Device, FC: Fiber Coupler, G: Galvanometer, PC: Polarization Control, RM: Reference Mirror, SL: Scan Lens.

Figure 1 shows the schematic of the combined OCT and LSFM system for embryonic imaging. The light blue section shows the OCT system, and light green section represents the LSFM system. We used 405 nm as the LSFM excitation wavelength, and detection was at 530 nm. The LSFM laser source (iChrome MLE, Toptica Photonics Inc., Munich, Germany) ran in

continuous mode, with an incident power on the sample of ~ 14 mW. After expanding the excitation beam, it was then directed to the galvanometer-mounted mirrors for scanning (GVS002, Thorlabs Inc., NJ) through the scan lens (LSM03-BB, Thorlabs Inc.,). The light sheet was generated by using one of the two scanning mirrors from the two-axis galvanometer, and the other axis was only used for precise alignment. The emission light was collected through a water immersion objective lens with 0.8 numerical aperture (N16LWD-PF, Nikon Corp., Tokyo, Japan) with a 3 mm working distance. The fluorescence signal passed through the objective lens, a filter (530 \pm 50 nm), and an infinity-corrected tube lens to the digital camera (C11440-22CU, Hamamatsu, Hamamatsu City, Japan).

The light green section of the schematic shows the swept-source OCT sub-system based on a swept source laser (1051 SSOCT, Axsun Tech., Billerica, MA) with a central wavelength of 1050 nm, scan range of 109 nm, and 100 kHz sweep rate. The OCT beam incident power on the sample was \sim 6 mW. The OCT beam was transmitted through a polarization beam splitter, where the OCT and LSFM excitation beams were combined. The OCT and LSFM excitation beams were aligned such that they were co-planar. An identical polarization beam splitter was placed in the reference arm to reduce the difference in dispersion between the reference arm and sample arm of the OCT system. The measured sensitivity of the OCT system was 100.1 dB, and the sensitivity roll-off over 4.13 mm was 6.9 dB. The OCT axial resolution was measured as 7.6 μ m in air. These LSFM and OCT beams were co-linear up to 3 mm, which was characterized by a beam viewer.

2.2 System characterization

Figure 2 shows the characterization of the multimodal system with a US air force resolution target, fluorescein solution, and fluorescent microspheres. Figures 2 (a) and (d) are images of the resolution target with the OCT and LSFM sub-systems., respectively. The measured LSFM transverse resolution was \sim 2.1 μ m, and the lateral resolution for the OCT system was \sim 14.9 μ m.

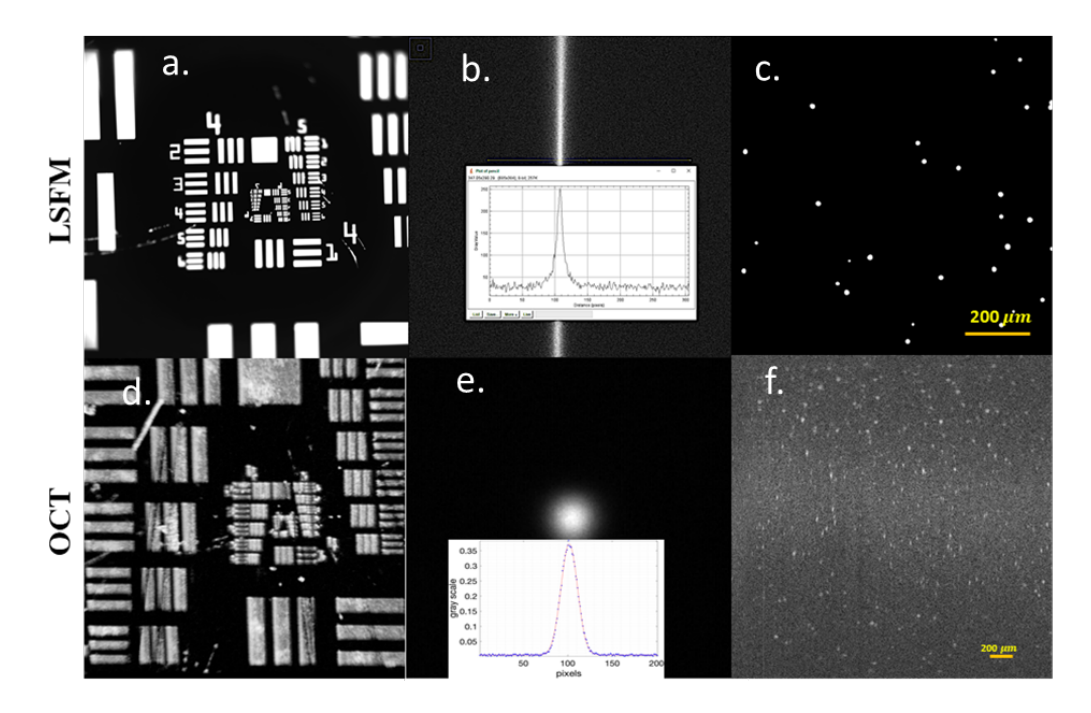


Figure 2. a) LSFM image of a US air force resolution target. b). LSFM excitation light pencil with a width of 13 um. c) LSFM image of 1-5 μ m microspheres. d) OCT image of the resolution target. e) OCT beam waist at focus. f) OCT image of the microspheres.

Figure 2(b) is an LSFM image of the light pencil (excitation beam with the scanners off) in a fluorescein solution demonstrating the light-sheet thickness (\sim 13.6 µm shown in the inset). Figure 2(e) shows an image of the OCT beam at the focus as captured by a beam viewer. A Gaussian fit of the beam profile showed a full width half maximum beam of 13 µm. Figures 2(c) and (f) are LSFM and OCT images of 1-5 µm diameter microspheres embedded in 1% agarose image, respectively. The image acquisition time was around \sim 0.6 s per 2D slice.

3. RESULTS

Figure 3 shows the LSFM and OCT images from the system. Here, 500 images were taken of a DAPI (4',6-diamidino-2-phenylindole) stained E9.5 embryo, and the step size was 5 μ m between images. Figures 3(a-c) clearly show the capability of the LSFM sub-system to image separate nuclei at the surface of the embryo and distinguish the different tissue types based on cellular density. For example, the epithelial tissue along the neural tube is obvious from the higher cellular density as compared to surrounding tissue. However, it can be easily seen that the penetration depth of the LSFM excitation beam is limited in the embryo as regions at the bottom of the image (LSFM excitation is from the top of the images) are blurry. Figures 3(a-c) are LSFM images at a depth 400 μ m, 450 μ m, and 575 μ m from the surface of the embryo facing the detection objective, respectively. In Figure 3(c), the LSFM image becomes blurry overall due to the scattering of the fluorescent emission through the embryo. Figures 3(d-f) are OCT images of the same embryo acquired concurrently with the LSFM images. OCT was able to image the entire embryo but with significantly reduced resolution and no molecular specificity.

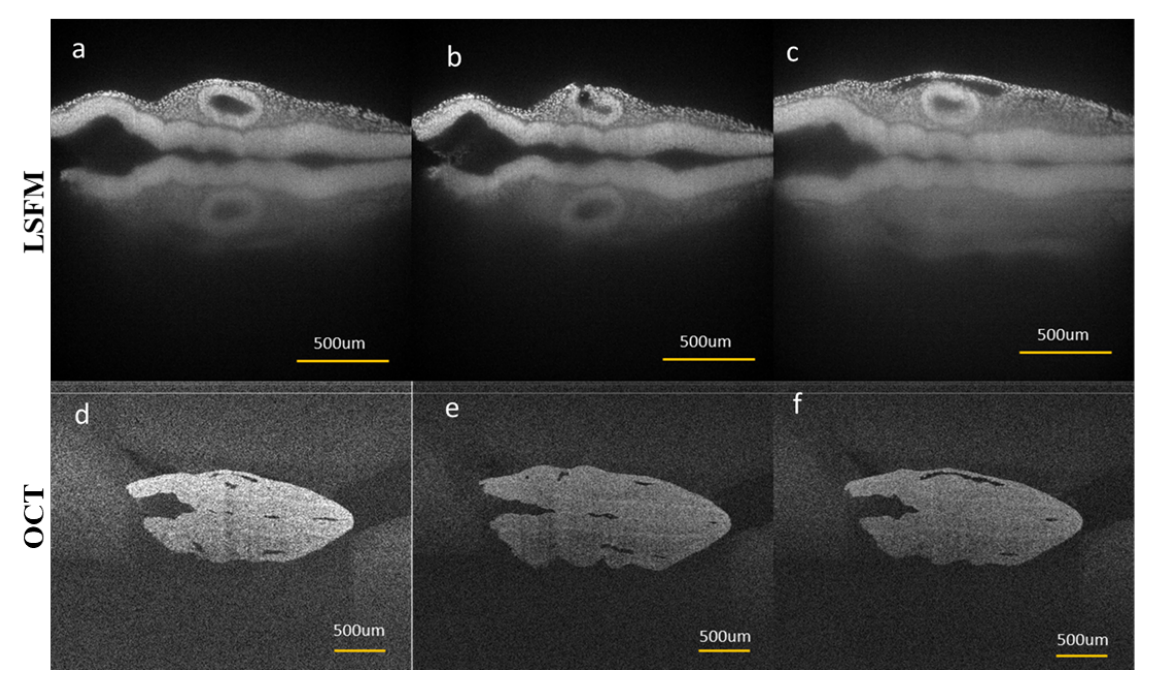


Figure 3. LSFM and OCT images of a DAPI-stained E9.5 murine embryo. a-c). LSFM images at different depths of E9.5 embryo. d-f) OCT images at the same corresponding depths acquired concurrently with the LSFM images.

Figures 4 (a, b) are 3D registered images of DAPI stained E9.5 embryo with combined OCT+LSFM system. The OCT and LSFM images were initially collected by our custom-built LabVIEW (NI, Austin, TX) interface. The raw OCT data was processed by MATLAB (Mathworks, Natick, MA), and 3D registration was displayed by using Amira (Thermo Fisher Scientific, Waltham, MA).

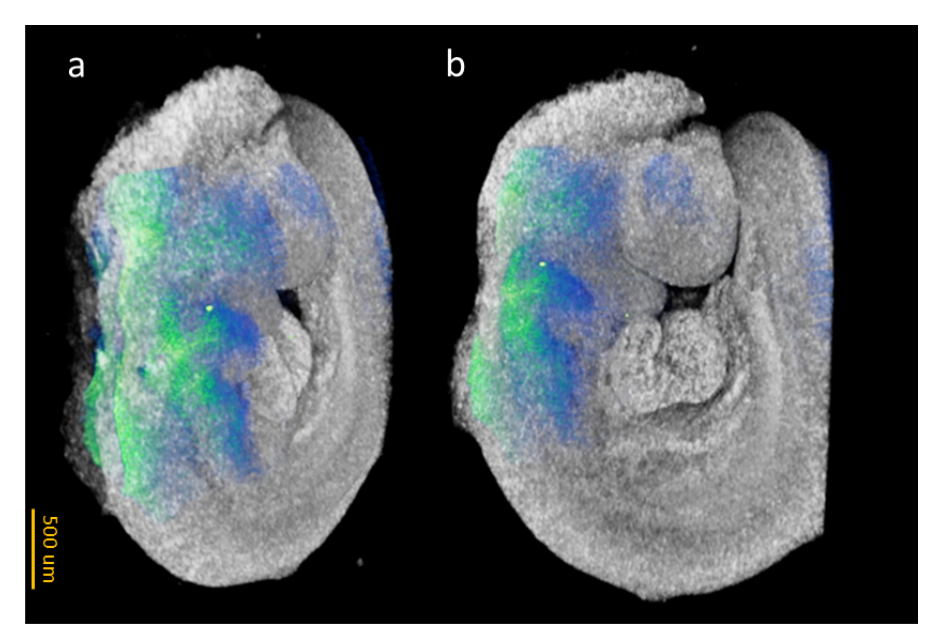


Figure 4. Combined 3D LSFM and OCT images of a DAPI-stained E9.5 murine embryo at (a) 45-degree rotation to the sagittal plane and (b) sagittal view.

4. DISCUSSION AND CONCLUSIONS

Our multimodal OCT and LSFM system acquired high-resolution structural and functional imaging at the same plane concurrently of murine embryos. Since the beams were co-planar, co-registration was trivial and reduced the computation complexity of post processing. However, there were several limitations of this multimodal system. For instance, the three-dimensional imaging acquisition speed was restricted by the LSFM acquisition time, and the sample was physically stepped with a translation stage to maintain the precise alignment of the LSFM excitation and detection arms. Although 3D OCT imaging is generally much faster with two-axis scanners, it was slower in this application by utilizing only one scanner in order to maintain co-planar imaging with LSFM. To maintain cellular-level resolution, the LSFM system has a limited field of view (~1.95 mm by ~1.95 mm), particularly compared to OCT imaging. The LSFM penetration depth was also limited for both excitation and detection. The next step of our work is to implement multiphoton excitation to overcome this limitation.

Funding. National Institutes of Health (P30EY007551, R01AA028406, R01HD096335, R01HL146745).

Disclosures. The authors declare no conflicts of interest

REFERENCES

- [1] N. E. Sharpless, and R. A. Depinho, "The mighty mouse: genetically engineered mouse models in cancer drug development," Nat Rev Drug Discov, 5(9), 741-54 (2006).
- [2] S. R. Montezuma, D. Vavvas, and J. W. Miller, "Review of the ocular angiogenesis animal models," Semin Ophthalmol, 24(2), 52-61 (2009).
- [3] C. Biben, R. Weber, S. Kesteven *et al.*, "Cardiac septal and valvular dysmorphogenesis in mice heterozygous for mutations in the homeobox gene Nkx2-5," Circ Res, 87(10), 888-95 (2000).
- [4] B. G. Bruneau, G. Nemer, J. P. Schmitt *et al.*, "A murine model of Holt-Oram syndrome defines roles of the T-box transcription factor Tbx5 in cardiogenesis and disease," Cell, 106(6), 709-21 (2001).

- [5] F. Cutrale, S. E. Fraser, and L. A. Trinh, "Imaging, Visualization, and Computation in Developmental Biology," Annual Review of Biomedical Data Science, Vol 2, 2019, 2, 223-251 (2019).
- [6] A. Greco, M. Mancini, S. Gargiulo *et al.*, "Ultrasound biomicroscopy in small animal research: applications in molecular and preclinical imaging," J Biomed Biotechnol, 2012, 519238 (2012).
- J. Sharpe, U. Ahlgren, P. Perry *et al.*, "Optical projection tomography as a tool for 3D microscopy and gene expression studies," Science, 296(5567), 541-5 (2002).
- [8] B. Hogers, D. Gross, V. Lehmann *et al.*, "Magnetic resonance microscopy of mouse embryos in utero," Anat Rec, 260(4), 373-7 (2000).
- [9] C. W. Hsu, L. Wong, T. L. Rasmussen *et al.*, "Three-dimensional microCT imaging of mouse development from early post-implantation to early postnatal stages," Dev Biol, 419(2), 229-236 (2016).
- [10] J. Fujimoto, and E. Swanson, "The Development, Commercialization, and Impact of Optical Coherence Tomography," Invest Ophthalmol Vis Sci, 57(9), OCT1-OCT13 (2016).
- J. Men, Y. Huang, J. Solanki *et al.*, "Optical Coherence Tomography for Brain Imaging and Developmental Biology," IEEE J Sel Top Quantum Electron, 22(4), (2016).
- [12] R. Raghunathan, M. Singh, M. E. Dickinson *et al.*, "Optical coherence tomography for embryonic imaging: a review," J Biomed Opt, 21(5), 50902 (2016).
- [13] S. Wang, M. Singh, A. L. Lopez, 3rd *et al.*, "Direct four-dimensional structural and functional imaging of cardiovascular dynamics in mouse embryos with 1.5 MHz optical coherence tomography," Opt Lett, 40(20), 4791-4 (2015).
- [14] J. Huisken, and D. Y. Stainier, "Selective plane illumination microscopy techniques in developmental biology," Development, 136(12), 1963-75 (2009).
- [15] R. M. Power, and J. Huisken, "A guide to light-sheet fluorescence microscopy for multiscale imaging," Nat Methods, 14(4), 360-373 (2017).
- [16] E. H. Stelzer, "Light-sheet fluorescence microscopy for quantitative biology," Nat Methods, 12(1), 23-6 (2015).